Research article

SURFACE and INTERFACE ANALYSIS

Received: 11 March 2014 Revised: 3 April 2014 Accepted: 6 April 2014 Published online in Wiley Online Library

(wileyonlinelibrary.com) DOI 10.1002/sia.5538

Influence of sputter power on structural and electrical properties of TiO_2 films for Al/TiO_2/Si gate capacitors

M. Chandra Sekhar,[a] N. Nanda Kumar Reddy,[a] B. Venkata Rao,[b] G. Mohan Rao[c] and S. Uthanna[b]*

Titanium dioxide (TiO_2) thin films were deposited onto p-Si substrates held at room temperature by reactive Direct Current (DC) magnetron sputtering at various sputter powers in the range 80–200 W. The as-deposited TiO_2 films were annealed at a temperature of 1023 K. The post-annealed films were characterized for crystallographic structure, chemical binding configuration, surface morphology and optical absorption. The electrical and dielectric properties of Al/TiO_2/p-Si structure were determined from the capacitance–voltage and current–voltage characteristics. X-ray diffraction studies confirmed that the as-deposited films were amorphous in nature. After post-annealing at 1023 K, the films formed at lower powers exhibited anatase phase, where as those deposited at sputter powers >160 W showed the mixed anatase and rutile phases of TiO_2. The surface morphology of the films varied significantly with the increase of sputter power. The electrical and dielectric properties on the air-annealed Al/TiO_2/p-Si structures were studied. The effect of sputter power on the electrical and dielectric characteristics of the structure of Al/TiO_2/p-Si (metal-insulator-semiconductor) was systematically investigated. Copyright © 2014 John Wiley & Sons, Ltd.

Keywords: sputtering; metal-insulator-semiconductor (MIS) structure; Schottky barrier height; ideality factor; series resistance

Introduction

Titanium dioxide (TiO_2) is a nontoxic oxide semiconductor drawn wide attention over the years because of its optical, photocatalytic and electronic properties. Because of its high dielectric constant and high resistivity, it attracted much attention for use in the fabrication of capacitors in microelectronic devices.[1] Campbell *et al.*[2] and Majewski *et al.*[3] explored the high dielectric properties of TiO_2 for its use as the gate dielectric in hole transporting p-channel thin film transistors. In addition, it is a potential candidate to replace the silicon dioxide as a gate dielectric in complementary metal oxide semiconductors because of its high dielectric constant.[4] Its photocatalytic property enables the application of TiO_2 films to environmental problems such as water decontamination processes, treatment of industrial effluents, air purification and destruction of microorganisms.[5] Also, because of its high chemical stability and modest bandgap, TiO_2 in thin film form are widely used as photocatalysts,[6] gas sensors[7] and dye-sensitized solar cells.[8]

Recently, the analysis of rectifying metal-semiconductor (MS) contacts (Schottky barrier diodes) is of prime interest for most of the elemental and compound semiconductors.[9,10] The earlier experimental results[11,12] of the Schottky barrier diodes revealed that the electrical characteristics of the devices strongly depend on the MS interface. It is well known that, unless specially fabricated, a Schottky barrier diode possesses a thin interfacial native oxide layer between the metal and the semiconductor. The presence of such an insulating layer converts the Schottky barrier diode into a metal-insulator-semiconductor (MIS) diode[13,14] that influences on the device electrical parameters.[14,15] Generally, the electronic properties of a Schottky diode are characterized by its main electrical parameters such as diode ideality factor, Schottky barrier height and series resistance, which provide useful information on the nature of the diode.[16] In recent years, Si Schottky diodes have received much attention, because of their maximum potential for high-power devices in novel band engineered heterostructure devices.[10,17]

TiO_2 is known to exist mainly in three crystalline forms namely anatase (A-tetragonal), rutile (R-tetragonal) and brookite (β-orthorhombic). Among these, anatase and rutile phases commonly exist in thin films of TiO_2. Anatase is a metastable phase exist at temperatures <873 K that transforms into highly stable rutile phase at temperatures >1073 K.[18] Anatase TiO_2 is potential for commercial used as photocatalyst because of its high photocatalytic activity. The rutile phase TiO_2 is extensively used as a dielectric layer for microelectronic applications. TiO_2 with a rutile structure is quite eccentric in terms of the dielectric constant among the other binary oxides. Brookite is the least stable of the three phases. The differences in assembly of titanium and oxygen atoms within the chains and in the lattice structures result in difference in band structure and bandgap (3.20 eV for anatase and 3.05 eV for rutile phase) of the TiO_2 in two phases.[19]

* *Correspondence to: U. Suda, Department of Physics, Sri Venkateswara University, Tirupati - 517 502, India.*
E-mail: chandu.phys@gmail.com

a *Department of Physics, Madanapalle Institute of Technology and Science, Madanapalle, 517 325, India*

b *Department of Physics, Sri Venkateswara University, Tirupati, 517 502, India*

c *Department of Instrumentation and Applied Physics, Indian Institute of Science, Bangalore, 560 012, India*

In the earlier works, TiO_2 thin films were deposited by a variety of methods such as sol–gel process,[20] thermal oxidation,[21] pulsed laser deposition,[22] chemical vapor deposition,[23] spray pyrolysis[24] and DC/Radio Frequency (RF) sputtering.[25–28] Among these methods, DC magnetron sputtering can produce highly uniform films with good adhesion to the surface of substrate. This method also offers the advantage of depositing films on large area substrates and on large scale that makes suitable for industrial applications. Physical properties of the sputter deposited films significantly depend on the sputter process parameters such as oxygen partial pressure, substrate temperature and substrate bias voltage fixed during the growth of the films. The post-deposition annealing also accelerates the crystal growth in turn influences the physical properties. In our earlier investigations, the films formed by DC magnetron sputtering of metallic titanium target at an oxygen partial pressure of 6×10^{-2} Pa were of stoichiometric TiO_2.[29] The TiO_2 films formed at substrate bias voltages greater than or equal to −150 V showed low leakage current and high dielectric constant and also correlated the variations in electrical transport properties with their structural and optical properties.[30] TiO_2 films formed at substrate temperatures ≥673 K exhibited high dielectric constant and also noticed an increase in the thickness of interfacial layer of SiO_2 layer thickness results in decrease in leakage currents. The growth of interfacial layer of SiO_2 between TiO_2 film and silicon substrate can be decreased by post-deposition annealing instead of deposition of TiO_2 films at elevated substrate temperatures. Hence, in the present investigation, an attempt is made to deposit TiO_2 films onto unheated p-type silicon substrate at various sputter posers. The as-deposited films were annealed in air at 1023 K and studied the influence of sputter power on the structural, electrical and dielectric properties.

Experimental techniques

Thin films of TiO_2 were deposited by DC reactive magnetron sputtering using titanium target (99.99% pure) of 100 mm diameter. The sputter chamber was evacuated to achieve an ultimate base pressure of 2×10^{-4} Pa using diffusion pump backed by rotary pump. The sputtering was performed in an atmosphere of argon and oxygen gas mixture. The films were deposited on the well cleaned p-type silicon (100) substrates held at room temperature (303 K) at a fixed oxygen partial pressure of 6×10^{-2} Pa and sputter pressure of 2×10^{-1} Pa at different sputter powers in the range 80–200 W. The as-deposited films were annealed in air for 1 h at 1023 K.

After deposition of the TiO_2 films, aluminum top electrodes (area (A) = 7.8×10^{-3} cm^2) were deposited on the deposited TiO_2 films using shadow mask. Thick platinum back contacts were made on Si using photolithography technique. High doping in Si ensures that this back contact would serve as ohmic. The thickness of the films was determined by Veeco Dektak depth profilometer (FTIR, NICOLET 5700 Thermo Electro Scientific INSTRUMENTS, LLC 5225 Varona Road Madison WI, 53711-4995, USA). The deposited films were characterized by studying their chemical binding configuration, crystallographic structure, surface morphology, and electrical and dielectric properties. The crystallographic structure of the films was studied with the X-ray diffractometer (Seifert model: 1003 TT Rich.Seifert and Co. Rontgenwerk, Bogenstrabe 41 D-22926, Ahrensburg Germany) in 2θ range 20–60° using $CuK_{\alpha1}$ radiation with wavelength of 0.15405 nm. The chemical binding configuration of the films was recorded with Fourier transform infrared spectroscope (Nicolet model 5700 FTIR) in the wavenumber range 400–4000 cm^{-1}. The surface morphology of the films was studied by atomic force microscopy (Veeco Instruments, Santa Barbara, CA). The electrical properties such as capacitance–voltage (C–V) and current–voltage (I–V) of the Al/TiO_2/p-Si capacitors were measured by using LCR meter (MIOKI model 3532-50) and Hewlett-Packard (model hp 4140B) pA meter (IISc, Bangalore), respectively.

Results and discussion

In order to study the influence of the sputtering power on the physical properties of TiO_2 films, the films were deposited under different sputtering powers in the range 80–200 W at the optimized oxygen partial pressure of 6×10^{-2} Pa using DC magnetron sputtering technique.[31] The thickness of the deposited films was measured with depth profilometer. The deposition rate was calculated from the thickness and duration of the deposition of the films. The dependence of deposition rate of the TiO_2 films on the sputter power is shown in Fig. 1. The deposition rate of the films at low sputter power of 80 W was 1.3 nm min^{-1}. The deposition rate of the films increased to 6.7 nm min^{-1} with the increase of sputter power to 200 W. At low sputter powers, the energy of the argon ions bombard the sputter target was low that leads to lower sputter yield hence of low deposition rate. At higher sputter powers, high argon ion flux bombardment on the target with high kinetic energy that will eject more atoms from the sputter target hence by increase in the deposition rate.

Figure 2 shows the X-ray diffraction profiles of the films formed at different sputtering powers. All the TiO_2 films deposited at room temperature (303 K) were of X-ray amorphous. In order to crystallize the films, the as-deposited films were annealed (T_a) in air at 1023 K. The films formed at low sputter power of 80 W and annealed at 1023 K showed the X-ray diffraction peaks at 2θ = 25.24°, 33.1°, 38.02° and 47.7° correspond to (101), (110), (004) and (200) reflections indicated the growth of TiO_2 with anatase phase.[32] It indicated that the films formed at 80 W and annealed in air at 1023 K contained smaller size crystallites with anatase phase of TiO_2 were embedded in the amorphous matrix. As the sputtering power increased to 120 W, in addition to these peaks, another diffraction peak at 27.3° related to the (110)

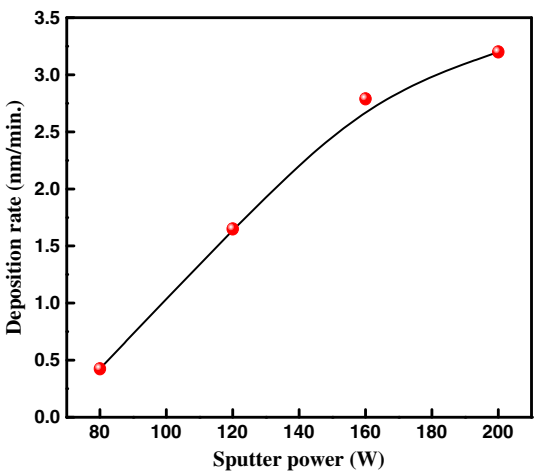

Figure 1. Variation of deposition rate with sputter power of TiO_2 films.

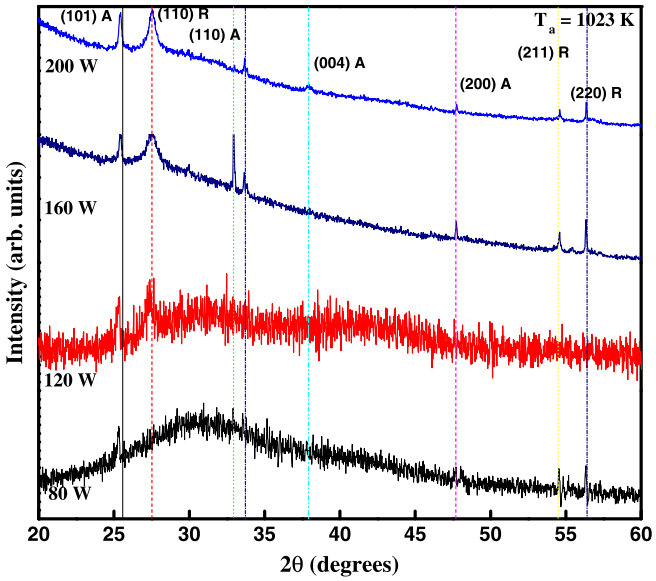

Figure 2. X-ray diffraction profiles of TiO_2 films formed at different sputter powers.

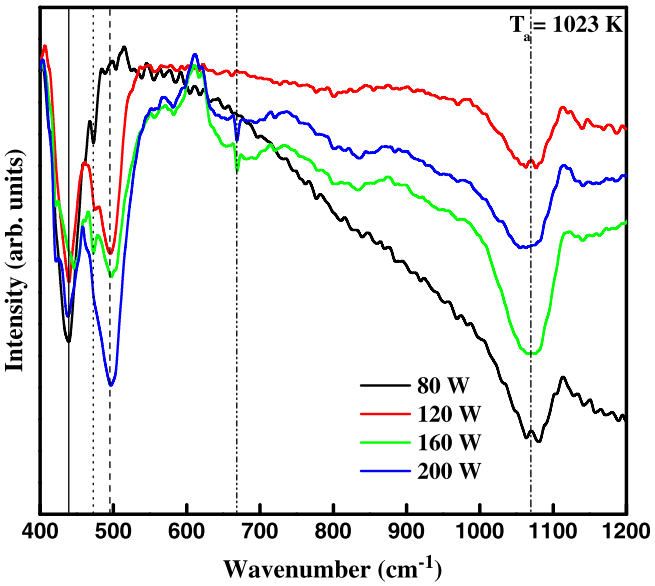

Figure 3. Fourier transform infrared transmittance spectra of TiO_2 films formed at different sputter powers.

reflection of rutile phase TiO_2 indicated the presence of mixed phase in the amorphous matrix.[33] The films formed at 160 W were of polycrystalline in nature with enhanced crystallite size as noticed by the increase in the intensity of the diffraction peaks. The intensity of the reflections (101) was decreased with the increase of sputter power from 120 to 200 W that indicated the decrease in anatase phase in the TiO_2 films. The full width at half maximum of (101) decreased with the increase of sputter power indicated the decrease in the crystallite size of anatase phase. The intensity of rutile (110) peak was increased and full width at half maximum decreased with the increase of sputter power from 120 to 200 W indicated the growth towards rutile phase at higher sputter powers. The crystallite size of the films was calculated from the diffraction peaks using Debye–Scherrer's relation

$$L = 0.89\,\lambda/\beta\cos\theta \quad (1)$$

Here, λ is the wavelength of the X-rays, β the full width at half maximum intensity of the diffraction peak and θ the Bragg diffraction angle. The crystallite size of the grown anatase TiO_2 films decreased from 40 to 20 nm with the increase of sputter power from 80 to 200 W, while the crystallite size of the rutile phase TiO_2 films increased from 10 to 30 nm with the increase of sputter power from 80 to 200 W.

Fourier transform infrared transmittance spectra (FTIR) of the annealed TiO_2 films deposited at different sputtering powers is shown in Fig. 3. The FTIR spectrum of the film deposited at low sputter power of 80 W showed a broad absorption band at 438 cm^{-1} related to the stretching vibration of Ti–O–Ti in anatase phase TiO_2.[34] When sputter power increased to 120 W, the absorption bands at 494 and 668 cm^{-1} were observed with minimum intensity. The bands situated at 494 and 668 cm^{-1} related to the rutile phase of TiO_2 with vibration modes of Ti–O–Ti.[35] Further, increase of sputter power to 160 W, the intensity of the bands at 494 and 668 cm^{-1} increased because of increase in the crystallinity of rutile phase in the films. The intensity of absorption band located at 438 cm^{-1} was decreased that indicated the decrease of the anatase phase TiO_2 with the increase of sputter power. These results were well supported by the X-ray diffraction studies.

Figure 4 shows the atomic force micrographs of the TiO_2 films deposited at different sputter powers. The micrographs showed that the TiO_2 films deposited at low sputter power of 80 W were of smoother and less dense in structure. At low sputter powers, the adatoms with low kinetic energy result in negligible surface diffusion. When sputter power increased to 120 W, the TiO_2 films appeared to be continuous with fine-sized grains might be due to the presence of mixed phase. Further, increase in sputter power to 160 W, the grain size of the films increased. The surface diffusion of the adatoms was enhanced with the momentum transfer to the growing surface resulted an increase in the grain size of the films. The enhancement in crystallinity of the films was achieved at higher sputter power of 200 W because of larger impact energy of the bombarding particles, which lead to better surface mobility. The higher the sputter power, the more likely the film formed were of continuous and with higher crystallinity due to sufficient high adatom mobility that improved the surface diffusion. The grain size of the TiO_2 films increased from 115 to 130 nm with the increase of sputter power from 80 to 200 W. Song *et al.*[36] reported that the increase in the grain size was a result of bombardment to the growth surface by more energetic particles with increase of sputter power.

Figure 5 shows the capacitance–voltage characteristic curves at different frequencies for Al/TiO_2/p-Si capacitors formed at different sputtering powers in the range 80–200 W and annealed at 1023 K. The capacitance of the TiO_2 capacitors was decreased with the increase in frequency. The high capacitance at low frequencies depends on the ability of the electron concentration to follow the applied signal. While the decrease in the capacitance at high frequencies, the charge at the interface cannot follow an Alternating Currents (AC) signal. The capacitance–voltage measurements on the TiO_2 films formed at different sputter powers and at fixed frequency of 1 MHz are shown in Fig. 6. The experimental characteristics are similar to the normal capacitance–voltage characteristics, where the charge accumulation, depletion and inversion could be easily recognized. For negatively biased structure, negative electron charge at the gate is balanced by positive hole charges accumulated near the surface of the semiconductor

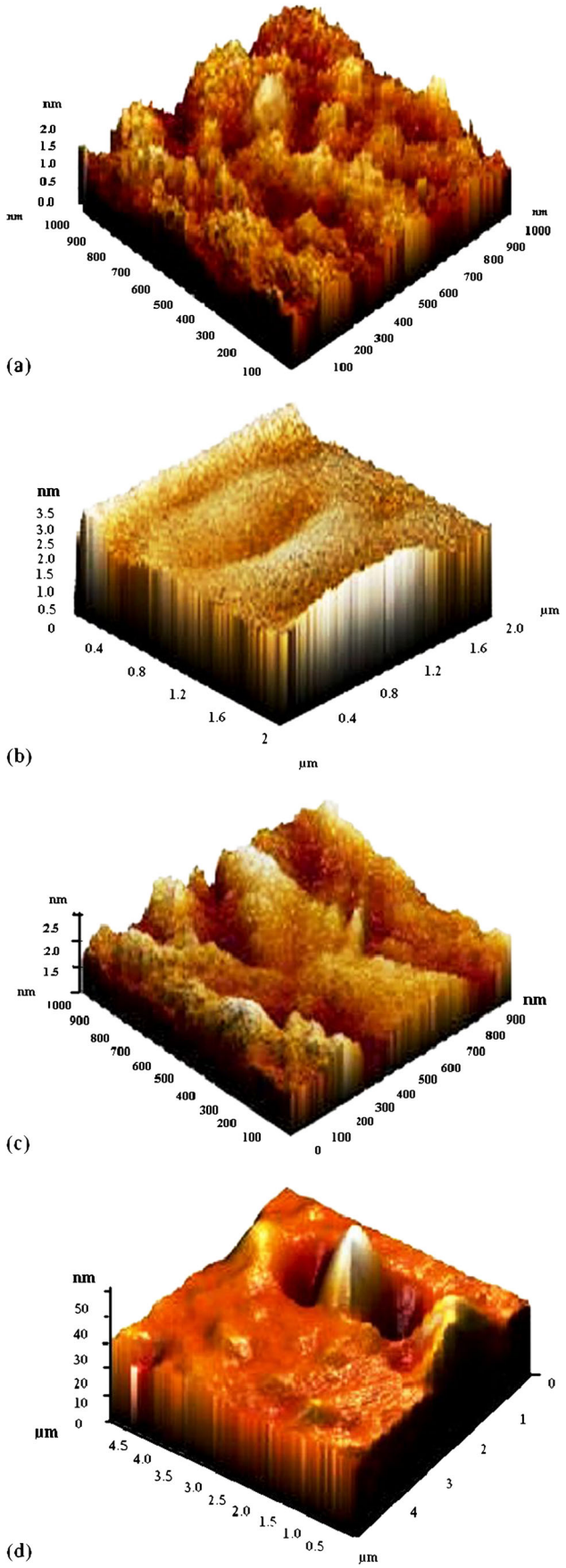

Figure 4. Atomic force micrographs of TiO_2 films formed at (a) 80, (b) 120, (c) 160 and (d) 200 W.

(p-type). In an ideal Metal-Oxide-Semiconductor (MOS) system, capacitance (C) measured in this accumulation state is equal to oxide capacitance $C_{ox} = 2.8$ nF at sputter power of 80 W. Switching the bias voltage into positive direction makes semiconductor surface depleted from the holes so that the additional capacitance of space charge layer C_s is series in connection with C_{ox}. Moreover, the positive gate biasing at low frequencies, an inversion in the type of conduction occurs. In the strong inversion conditions, potential changes at the gate are determined by the presence of electrons at the semiconductor metal interface. Thus, the total measured capacitance, similar to the accumulation state, approaches to the C_{ox}. The capacitance of TiO_2 films was decreased from 2.8 to 1.3 nF with the increase of sputter power from 80 to 200 W. Such a decrease in the capacitance with the increase of sputter power was also noticed by Huang *et al.*[37] At low sputter powers, the capacitance of the TiO_2 capacitors was high because of the low thickness of the films. From the measured capacitance and the physical thickness (t), the dielectric constant (k) of the TiO_2 capacitor can be calculated. The dielectric constant (k) of the films was calculated from the capacitance–voltage curves using the following relations:

$$C = k\varepsilon_o A/t \tag{2}$$

where C is the capacitance, k the dielectric constant of the material, ε_o the permittivity of free space (8.85×10^{-3} fF μm^{-1}) and A the area of the capacitor. The dielectric constant of the TiO_2 films formed at sputter power of 80 W was 10, and it increased to 30 with the increase of sputtering power to 200 W. The dielectric constant of the films increased with the increase of sputter power. The annealing of films formed at different sputter powers leads to decrease of structural defects and the change of the phase transformation from anatase to rutile phase, hence enhance in the dielectric constant of the TiO_2 films.

Figure 7 shows the forward and reverse current–voltage characteristics of the MIS (Al/TiO_2/p-Si) structured capacitors formed at different sputter powers for negative and positive applied voltages. For the current–voltage measurements, a step time of 1 s and a step voltage of 0.1 V were used. It is seen in Fig. 7 that the leakage current increased with the increase of sputter power. The minimum leakage current achieved for sputter power of 80 W at a gate bias voltage of 1.5 V was 6.38×10^{-10} A and it was increased to 9.0×10^{-7} A by increase of sputter power to 200 W. The increase in leakage current density with sputtering power was due to the increase in oxygen defects in the TiO_2 films and also increases in the structural defects. Such an increase in leakage currents with the increase in sputter power was also observed in $MgTiO_3$ films formed by DC/RF sputtering.[37]

Moreover, we made an attempt to study the effect of sputtering power on Schottky barrier parameters such as Schottky barrier height (Φ_b), ideality factor (n) and series resistance (R_S) from the forward and reverse I–V characteristics of Al/TiO_2/p-Si device (Fig. 7). The forward I–V characteristics were analyzed by using thermionic emission relation for electron transport from a metal/semiconductor is given by the relation[13]

$$I = I_0 \exp\left(\frac{qV}{nkT}\right)\left[1 - \exp\left(\frac{-qV}{kT}\right)\right] \tag{3}$$

and

$$I_o = AA^{**}T^2 \exp\left(\frac{-q\Phi_b}{kT}\right) \tag{4}$$

where I_o is the saturation current, q the electronic charge, A^{**} the effective Richardson's constant that is 32 A cm^{-2} K^2 for p-Si,[17] k

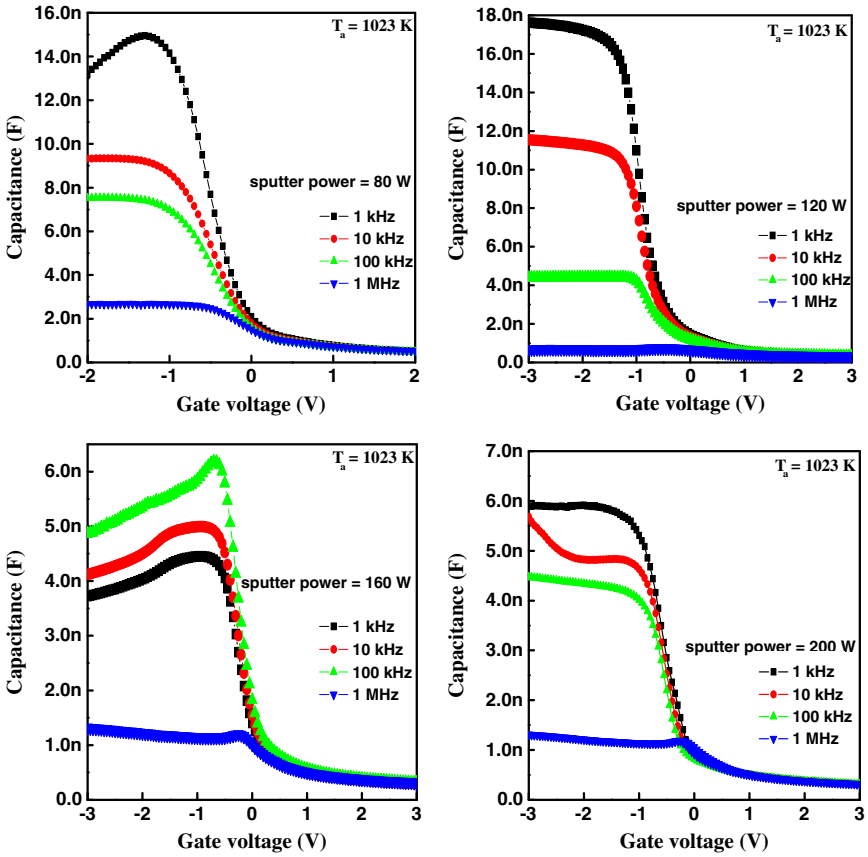

Figure 5. Capacitance–voltage curves of Al/TiO_2/p-Si capacitors at different frequencies.

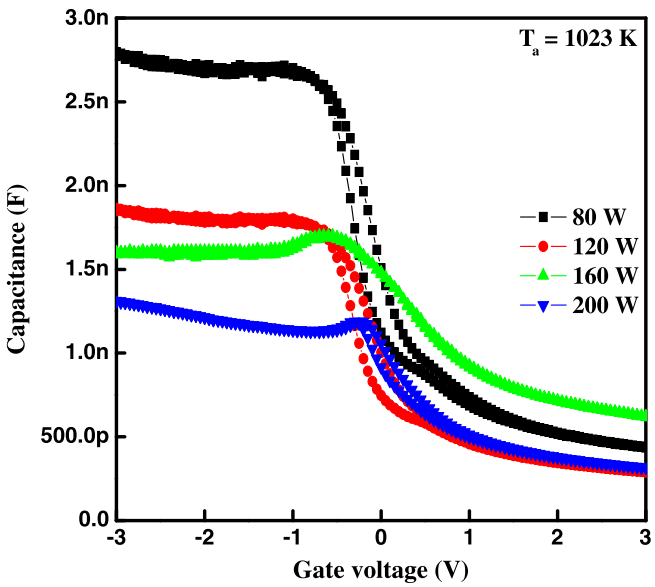

Figure 6. Capacitance–voltage curves (at 1 MHz) of Al/TiO_2/p-Si capacitors at different sputter powers.

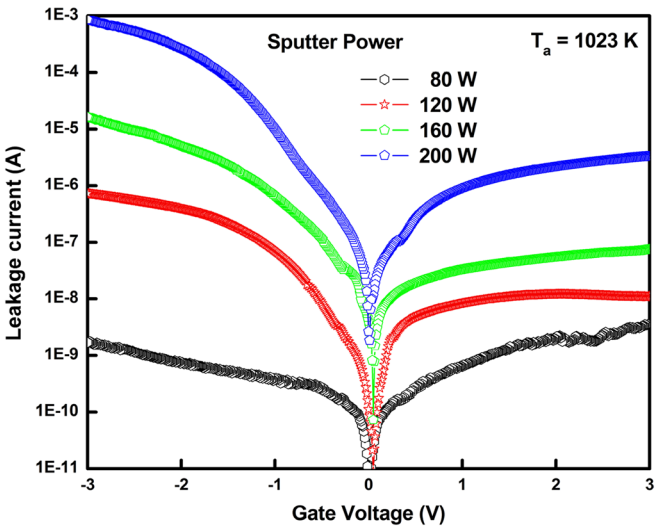

Figure 7. Current–voltage characteristics of TiO_2 films formed at different sputter powers.

is the Boltzmann's constant and n the ideality factor. The ideality factor is calculated from the slope of the linear region of the forward-bias ln$I$ versus V plots using Equation (4) as

$$n = \frac{q}{kT}\left(\frac{dV}{d(\ln I)}\right) \tag{5}$$

The Schottky barrier height (Φ_b) is determined from the relation

$$\Phi_b = \frac{kT}{q}\ln\left(\frac{AA^{**}T^2}{I_0}\right) \tag{6}$$

Using linear curve fitting for the forward characteristics of ln$I$ versus V data, the barrier height and ideality factor can

be determined from the *y*-axis intercept and the slope of the fitted curves, respectively.

Calculations indicated that the Schottky barrier height of the Al/TiO_2/p-Si structure is found to be 0.71 eV for the TiO_2 film deposited at 200 W. The estimated Schottky barrier heights of contacts are 0.76 eV for 160 W, 0.84 eV for 120 W and 0.87 eV for 80 W. Thus, it is observed that the Schottky barrier height increased from 0.71 to 0.87 eV with a decrease in the sputter power from 200 to 80 W. The barrier height extracted for the TiO_2 film deposited at 200 W is similar to that reported by Pakma *et al.*[10] for Al/TiO_2/p-Si structure.

The calculated ideality factor for the TiO_2 film deposited at 200 W is found to be 3.76. However, the ideality factor decreases to 1.27 at sputter power 80 W. The ideality factor (*n*) values greater than unity can be ascribed to the effects of the bias voltage drop across the interfacial insulator layer, the distribution of interface states at the insulator/semiconductor interface and the barrier inhomogeneities prevailing at the metal/semiconductor interface.[38,39] The variation of barrier height and ideality factor values with sputter power for the Al/TiO_2/p-Si structure is shown in Fig. 8.

Figure 9 shows the plots of experimental $dV/d\ln I$ versus *I* for different sputter powers. The ln*I*–*V* curves are generally no longer a straight line at voltages in excess of 0.25 V. The reason for the deviation of forward bias *I*–*V* curves from the linearity could be due to the effect of series resistance (R_S), the interfacial insulator layer and the interface state density when the applied voltage is sufficiently large.[40] The series resistance values are obtained from the forward-bias *I*–*V* curves using the method developed by Cheung and Cheung.[41] The forward bias current–voltage characteristics due to thermionic emission of a Schottky contact with the series resistance can be expressed as Cheung's function

$$\frac{dV}{d(\ln I)} = IR_S + n\left(\frac{kT}{q}\right) \tag{7}$$

The values of series resistance of Al/TiO_2/p-Si structure were calculated from the plots of $dV/d\ln I$ versus *I*. The extracted values of R_S for Au/TiO_2/p-Si structure were changed from 14.8 to 2.57 MΩ at 80 and 200 W, respectively, and the series resistance (R_S) values are tabulated in Table 1.

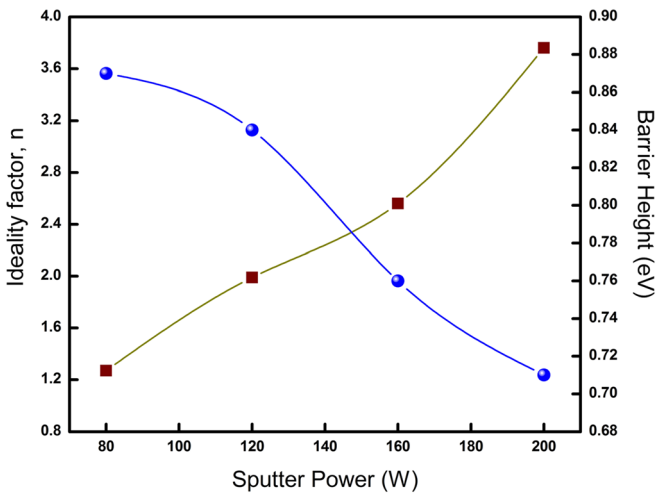

Figure 8. The barrier height versus ideality factor as a function of sputter power for Al/TiO_2 /p-Si structure.

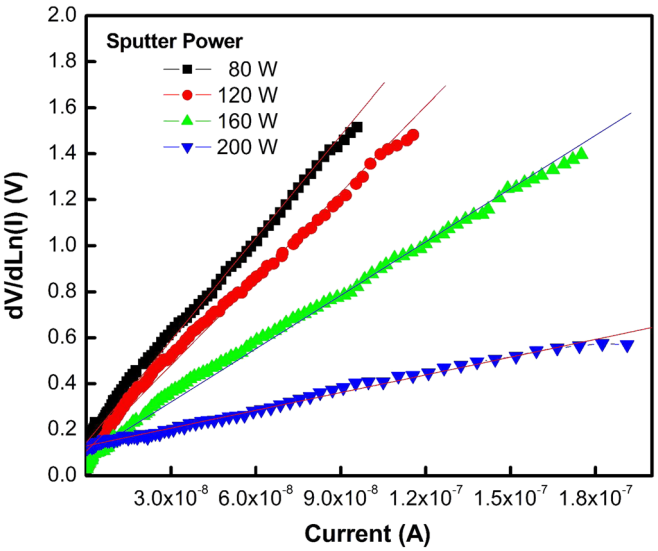

Figure 9. The experimental $dV/d\ln(I)$ versus *I* plot obtained from forward bias current–voltage characteristics (Fig. 7) of the Al/TiO_2 /p-Si structure.

Table 1. Variation of electrical parameters of Al/TiO_2/p-Si structure obtained using current–voltage characteristics

Sputter power (W)	Leakage current (*A*) (at 1.5 V)	Barrier height (eV)	Ideality factor (*n*)	Series resistance (MΩ)
80	6.38×10^{-10}	0.87	1.27	14.8
120	8.26×10^{-9}	0.84	1.99	12.5
160	3.29×10^{-8}	0.76	2.56	7.77
200	9.0×10^{-7}	0.71	3.76	2.57

Conclusion

TiO_2 thin films have been deposited by using DC magnetron sputtering of titanium target onto unheated quartz and p-silicon substrates at an oxygen partial pressure of 6×10^{-2} Pa and at different sputtering powers in the range 80–200 W. The deposition rate of the films was increased with the increase of sputter power. The effect of sputter power on structural, electrical and dielectric and optical properties of the air-annealed films was studied. The structural properties were determined by using X-ray diffraction, and FTIR studies. All the as-deposited were of X-ray amorphous. The structural analysis of the annealed films revealed that the films formed at low sputter power of 80 W showed anatase phase, while those deposited at higher sputter powers ≥160 W were exhibit-mixed phase of anatase and rutile. The crystallite size of the films increased with the increase of sputter power. The surface roughness of the thin films increased with the sputter power as revealed by Atomic Force Microscopy (AFM). The electrical and dielectric properties of the Al/TiO_2/p-Si stacks were studied by using *C*–*V* and *I*–*V* measurements. The dielectric constant of the TiO_2 films was increased from 10 to 30 with the increase of sputter power from 80 to 200 W. The formed capacitors exhibited Schottky emission at lower electric fields. Also, the influence of sputtering power on the electrical characteristics of Al/TiO_2/p-Si (MIS) structure has been reported in the range 80–200 W.

Acknowledgements

This work was carried out with the financial support of the University Grant Commission, New Delhi, India, through a sanctioned Major Research Project: F. No. 34-36/2008 (SR) dated 30-12-2008. One of the authors, M. Chandra Sekhar, is thankful to the University Grants Commission, New Delhi, for the award of UGC-RFSMS fellowship.

References

[1] H. Poelman, D. Poelman, D. Depla, H. Tomaszewski, L. Fiermans, R. De Gryse, *Surf. Sci.* **2001**, *485*, 482.
[2] S. A. Campbell, D. C. Gilmer, W. X. Chuan, H. M. Ta, K. H. Seag, W. L. Gladfelter, Y. Jinhua, *IEEE Trans. Electron Dev.* **1997**, *44*, 104.
[3] L. A. Majewski, R. Schroeder, M. Grell, *Adv. Funct. Mater.* **2005**, *15*, 1017.
[4] S. Kundu, S. Kumar Roy, P. Banerji, *J. Phys. D Appl. Phys.* **2011**, *44*, 155104.
[5] M. R. Hoffmann, S. T. Martin, W. Choi, D. W. Bahnemann, *Chem. Rev.* **1995**, *95*, 69.
[6] V. Senthil Kumar, M. Jayachandran, C. Sanjeevaraja, *Thin Solid Films* **2010**, *519*, 991.
[7] A. R. Armstrong, G. Armstrong, J. Canales, R. Garcia, P. G. Bruce, *Adv. Mater.* **2005**, *17*, 862.
[8] Y. M. Sung, H. J. Kim, *Thin Solid Films* **2007**, *515*, 4996.
[9] M. Jang, Y. Kim, J. Shin, S. Lee, *IEEE Electron. Dev. Lett.* **2005**, *26*, 354.
[10] O. Pakma, N. Serin, T. Serin, S. Altındal, *J. Appl. Phys.* **2008**, *104*, 014501.
[11] A. Sing, K. C. Reinhardt, W. A. Anderson, *J. Appl. Phys.* **1990**, *68*, 3475.
[12] S. Chand, S. Bala, *Physica B* **2007**, *390*, 179.
[13] E. H. Rhoderick, R. H. Williams, Metal Semiconductor Contacts, Clarendon Press, Oxford University Press, New York, **1988**.
[14] M. E. Aydin, K. Akkilic, T. Kilicoglu, *Physica B* **2004**, *352*, 312; 2006 *Appl. Surf. Sci.* **253** 1304.
[15] A. Motayed, S. N. Mohammad, *J. Chem. Phys.* **2005**, *123*, 194703.
[16] B. Kinaci, T. Asar, Y. Özen, S. Özcelik, *Optoelectron. Adv. Mater. Rapid Commun.* **2011**, *5l*, 434.
[17] M. E. Aydın, O. Gullu, N. Yıldırım, *Physica B* **2008**, *403*, 131.
[18] M. D. Wiggins, M. C. Neison, C. R. Aita, *J. Vac. Sci. Technol. A* **1996**, *14*, 772.
[19] A. K. Sharma, R. K. Thareja, U. Willer and W. Schade, *Appl. Surf. Sci.* **2003**, *206*, 137.
[20] C. Anderson, A. J. Bard, *J. Phys. Chem.* **1995**, *99*, 9882.
[21] L. H. Cong, K. Mallik, C. H. de Groot, R. Kersting, *J. Phys.: Condens. Mater* **2006**, *18*, 645.
[22] E. Györgya, G. Socola, E. Axentea, I. N. Mihailescua, C. Ducub, S. Ciucac, *Appl. Surf. Sci.* **2005**, *247*, 429.
[23] Y. Masuda, Y. Jinbo, K. Koumoto, *Sci. Adv. Mater.* **2009**, *1*, 138.
[24] P. H. Wöbkenberg, T. Ishwaral, J. Nelson, D. D. C. Bradley, S. A. Haque, T. D. Anthopoulos, *Appl. Phys. Lett.* **2010**, *96*, 082116.
[25] M. N. Islam, T. B. Ghosh, K. L. Chopra, H. N. Acharya, *Thin Solid Films* **1996**, *280*, 20.
[26] C. B. Heo, J. H. Boo, *Thin Solid Films* **2005**, *475*, 183
[27] P. Kondaiah, M. Chandra Sekhar, G. Mohan Rao, S. Uthanna, *Sci. Adv. Mater.* **2013**, *5*, 398.
[28] T. Minami, H. Sato, K. Ohashi, T. Tomofugi, S. Takata, *J. Cryst. Growth* **1992**, *117*, 370.
[29] M. Chandra Sekhar, P. Kondaiah, B. Radha Krishna, S. Uthanna, *J. Spectroscopy* **2013**, *2013*, **ID 462734**, Doi: 10.1155/2013/462734.
[30] M. Chandra Sekhar, P. Kondaiah, S. V. Jagadeesh Chandra, G. Mohan Rao, S. Uthanna, *Appl. Surf. Sci.* **2011**, *258*, 1789.
[31] M. Chandra Sekhar, P. Kondaiah, S. V. Jagadeesh Chandra, G. Mohan Rao, S. Uthanna, *Surf. Inteface Anal.* **2012**, *44*, 1299.
[32] JCPDS, International Center for Diffraction Data, card No. 084-285.
[33] G. He, Q. Fang, L. Zhu, M. Liu, L. Zhang, *Chem. Phys. Lett.* **2004**, *395*, 259.
[34] K. F. Albertin, I. Pereyra, *Thin Solid Films* **2009**, *517*, 4548.
[35] S. Duenas, H. Castan, H. Garcia, E. San Andreas, M. T. Luque, I. Martil, G. G. Diaz, K. Kukli, T. Uustare, J. Aarik, *Semicond. Sci. Technol.* **2005**, *20*, 1044.
[36] Y. S. Song, J. K. Park, T. W. Kin, C. W. Chung, *Thin Solid Films* **2004**, *467*, 120.
[37] C. L. Huang, Y. B. Chen, *J. Cryst. Growth* **2005**, *285*, 586.
[38] S. Altındal, İ. Dökme, M. M. Bülbül, N. Yalçın, T. Serin, *Microelectron. Eng.* **2006**, *83*, 499.
[39] S. Chand, J. Kumar, *Semicond. Sci. Technol.* **1996**, *11*, 1203.
[40] H. Altuntas, A. Bengi, T. Asar, U. Aydemir, B. Sarıkavak, Y. Ozen, S. Altındal, S. Ozcelik, *Surf. Interface Anal.* **2010**, *42*, 1257.
[41] S. K. Cheung, N. W. Cheung, *Appl. Phys. Lett.* **1986**, *49*, 85.